Pure Conducting Polymer Hydrogels Increase Signal-to-Noise of Cutaneous Electrodes by Lowering Skin Interface Impedance

Sebastian Roubert Martinez, Paul Le Floch, Jia Liu, Robert D. Howe*

S. Roubert Martinez, Dr. P. Le Floch, Prof. J. Liu, Prof. R.D. Howe
John A. Paulson School of Engineering and Applied Sciences
Harvard University
150 Western Avenue, Boston, MA 02134
Email Address: howe@seas.harvard.edu

Keywords: *hydrogels, conductive polymers, bioelectronics, skin, neural interfaces*

Cutaneous electrodes are routinely used for noninvasive electrophysiological sensing of signals from the brain, the heart, and the neuromuscular system. These bioelectronic signals propagate as ionic charge from their sources to the skin-electrode interface where they are then sensed as electronic charge by the instrumentation. However, these signals suffer from low signal-to-noise ratio arising from the high impedance at the tissue-to-electrode contact interface. This article reports that soft conductive polymer hydrogels made purely of PEDOT: PSS present nearly an order of magnitude decrease in the skin-electrode contact impedance (88%, 82%, and 77% at 10Hz, 100Hz, and 1kHz, respectively) when compared to clinical electrodes in an *ex-vivo* model that isolates the bioelectrochemical features of a single skin-electrode contact. Integrating these pure soft conductive polymer blocks into an adhesive wearable sensor enables high fidelity bioelectronic signals with higher signal-to-noise ratio (average 2.1dB increase, max 3.4dB increase) when compared to clinical electrodes across all subjects. The utility of these electrodes is demonstrated in a neural interface application. The conductive polymer hydrogels enable electromyogram-based velocity-control of a robotic arm to complete a pick and place task. This work provides a basis for the characterization and use of conductive polymer hydrogels to better couple human and machine.

1   Introduction

Cutaneous electrodes enable noninvasive electrophysiological sensing of the human body, for applications that include the heart (electrocardiography, ECG), the brain (electroencephalography, EEG), and the neuromuscular system (electromyography, EMG)[1]. Signal-to-noise ratio (SNR) is critical since signals are small and measurements are susceptible to environmental noise, baseline drift, and contamination from other electrophysiological signals, e.g. ECG signal contaminating EMG signal[2],[3],[4]. Problems arise when skin-electrode impedance is both high and variable at the recording and the reference electrode sites [5]. Thus, electrode materials possessing low skin-electrode impedance across skin sites are needed to reduce noise sensitivity and ensure high quality signal acquisition. Flexibility and conformation to the skin are also important to minimize motion artefacts due to impedance variation[6].

A key aspect of minimizing impedance is to reduce the disparity between bioconduction using ions and instrumentation conduction using electrons [1]. The clinical and research standard for cutaneous electrodes has been the Ag/AgCl electrode coupled with an electrolytic gel to accommodate ionic conduction
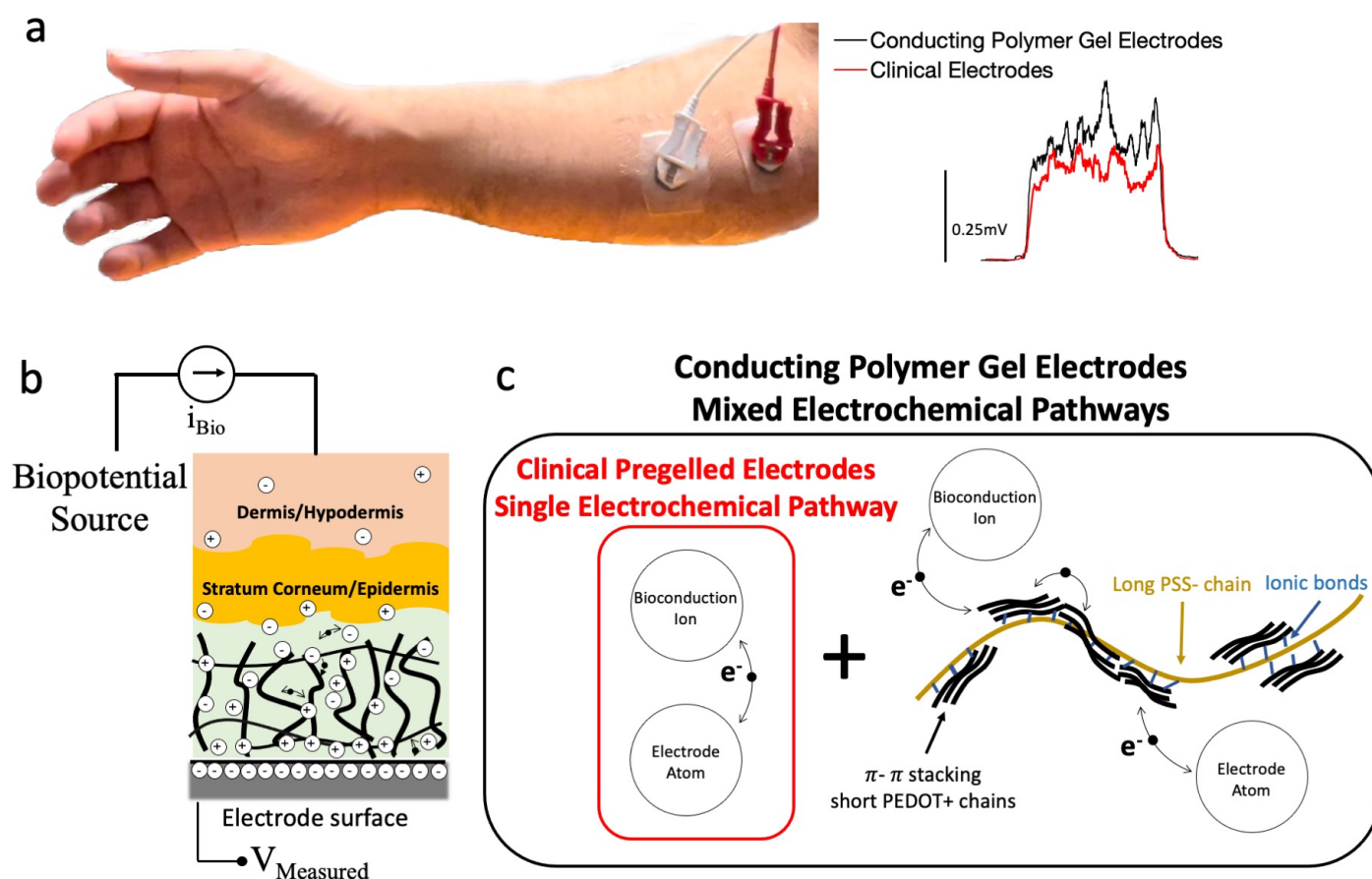

Figure 1: Conductive polymer hydrogels as cutaneous electrodes. a) (Left) Example placement on a human forearm. (Right) Example electromyographic signals comparing electrodes used in the clinic/market to conductive polymer (CP) hydrogel electrodes. b) Biopotential signals propogate as ions from deep tissue, from the skin, as a mix of ions and electrons throughout the volume of the conductive polymer gel, and finally as electrons to the electrode surface for instrumentation recording. c) Schematic illustration of the mixed electrochemical pathways (i.e., Faradaic reactions) of a conductive polymer gel. CP gel chemistry: PEDOT+ chains ionically bond to PSS- chains, long PSS- chains enable mechanical stretchability and stability of the gel, π-π stacking of PEDOT+ chains enable local electronic conductivity. The CP gels contain a percolated network of PEDOT+ chains for global conductivity throughout the CP gel to transfer charge to the electrode surface.

by interfacing with the porous nature of skin[1],[7]. The electrode is rigid, limiting full conformation of the skin and leading to motion artefacts. Many recent works apply new materials to create higher performing and more versatile electrodes. In particular, titanium carbide ($Ti_3C_2T_x$) MXene[8] presents excellent impedance, almost an order of magnitude lower than a commercial standard at 10Hz, and flexibility for skin conformability. Stauffer et al.[9] reported a soft, dry porous silver polymer electrode exhibiting greater than 30% mean impedance decrease over the clinical standard from 1Hz to 100Hz. Yao et. al. developed an ultrasoft silver nanoparticle (AgNP) elastomer hybrid for electromyography and robotic control [10]. However, these materials are limited by some combination of high stiffness (MXene, 330 GPa[11], mechanical impedance mismatch for movements with high skin stretch), complex specialized manufacturing processes (ion-etching MXene[8], microscale techniques for silver polymer electrodes[9]), or little improvements over the commercially available pregelled electrodes (Yao et. al.[10] reported lower impedance compared to clinical electrodes only up to 10Hz, at the bandwidths necessary for EMG and ECG they matched impedance to commercial electrodes).

Other promising approaches use the conductive polymer poly(3,4-ethylenedioxy-thiophene) doped with poly(styrene sulfonate) (PEDOT:PSS). Textile PEDOT electrodes promise conformability, flexibility, and the potential for integration into clothing. However, performance outcomes are lower than commercial electrodes: higher skin-electrode impedance, higher noise, and more drift[5],[12]. Other attempts to utilize PEDOT as a cutaneous electrode use thin films[13],[14],[15]. However, while these devices exhibit flexibility, stretchability is constrained by stiff substrates, limiting their general use for EMG applications [13],[14]. Nagamine et. al[15] developed a stretchable electrode device with Au as the backing layer of a PEDOT:PSS film and displayed 20% strain. However, the fabrication technique required 5um-scale precision using photolithography, limiting scalability and dissemination. Recent promising efforts focus on making intrinsically adhesive PEDOT:PSS films[16],[17],[18] for intimate contact to human skin and artifact reduction but yield skin impedance performance comparable to commercially-available electrodes. A possible approach for cutaneous bioelectronic sensing is to use the increased ionic conduction offered by hydrogels to augment the mixed conduction of these conductive polymers. Historically, studies of PE DOT:PSS and its gel form focus on invasive electrophysiological sensing including the human brain[19],[20],[21],[22],[23] In the past few years, PEDOT-based[24],[25],[26],[27],[28],[29],[30] and other conducting polymer (CP)[31],[32],[33],[34] composite hydrogels illustrate promising applications in non-invasive human electrophysiology *in-vivo*. However, previous work along these lines demonstrate skin impedance comparable to the clinical standards (Supplementary Table 1).

In this work, we present the use of a pure conductive polymer hydrogel, specifically the pure PEDOT:PSS hydrogel[35], as a cutaneous electrode on the human. The PEDOT:PSS gel, as both an excellent ionic and electronic conductor[35], serves as an ideal interface between ionic conduction in the skin and electronic conduction in the instrumentation. The use of the pure PEDOT:PSS hydrogel (where the use of a secondary dopant is added to increase conductivity in initial synthesis then removed to yield a pure PEDOT:PSS hydrogel network where high conductivity is preserved) provides significantly reduced skininterface impedance compared to previously published work using PEDOT:PSS-based hydrogels on humans *in-vivo* (Supplementary Table 1). As seen in **Figure 1**, the porous gel conforms to the skin and allows for electrochemical reactions throughout the gel (in contrast to only at the planar electrode interface for conventional electrodes), leading to the excellent skin-contact impedance compared to clinical electrodes in **Figure 2**. We surround the gel with soft adhesive elastomeric structures to form a wearable adhesive sensor and display an increase in the signal-to-noise ratio (SNR) when compared to clinical electrodes (**Figure 3**). Isolating skin-electrode tissue interface shows why this material leads to superior performance: this manuscript is first to demonstrate a method that isolates the electrochemical features at a single skin-

electrode contact, see Figure 2a for setup. Finally, to demonstrate the benefits of the conductive polymer hydrogel in an integrated bioelectronic system, we use the wearable adhesive conductive polymer hydrogel sensor to enable sensitive real-time teleoperated myoelectric velocity control of a robot arm in a commonplace activity of daily living: pick-and-place (Supplementary Video 1, **Figure 4**).

2 Results and Discussion

2.1 Single Site Skin-Electrode Contact Electrochemical Characterization

To characterize the utility of the pure PEDOT:PSS gel for wearable electrophysiological sensing, we first verify that the PEDOT:PSS gel improves the state of the art by directly comparing the PEDOT:PSS gel to the clinical standard pregelled Ag/AgCl electrode using state-of-the-art electrochemical characterization techniques, specifically electrochemical impedance spectroscopy (EIS) and cyclic voltametry (CV).

Standard methods to quantify skin-electrode electrode impedance use either a 2- or 3-electrode potentiostat setup[5],[8],[12],[36],[37],[38],[39],[40]. In the 3-electrode setup, the electrode material of study is used as the working electrode with usually a pregelled commercial electrode as the reference electrode and counter electrode. In the 2-electrode setup, the electrode material of interest is used as both the working and counter electrode. These methods give insight on electrochemical impedance trends and correlate well with SNR, especially if the electrode material of interest far outperforms clinical standard electrodes. However, their underlying analysis assumes that skin electrical properties are the same at all 2or 3-electrode sites despite electrochemical properties of skin sites varying widely with factors such as density of sweat glands[41],[5],[42],[43].

We take advantage of porcine skin's widespread use as a pre-clinical *ex-vivo* model[44],[45],[46],[47] to isolate the single skin-electrode contact with a novel setup in Figure 2a, enabling isolated EIS and CV that controls for skin sites and study only the effects of changing the interfacial material.

2.1.1 Impedance Measurements

We performed EIS in the frequency range of $0.1\text{-}10^5$Hz across three different electrodes: pregelled (electrolytic gel) clinical electrodes (Ag/AgCl electrodes, Noraxon), clinical electrodes with the electrolytic gel removed (bare metal), and the pure conductive polymer hydrogel (PEDOT:PSS gel). The PEDOT:PSS gel results has lower impedance across all frequencies (Figure 2b, top) compared to electrolytic gel and bare cases along with an increase in corner frequencies corresponding to less capacitive behavior (Figure 2b, bottom). At critical bioelectronic frequencies for cutaneous applications (Figure 2c), the use of PEDOT:PSS gel leads to significant reductions in skin-electrode contact impedance compared to the electrolytic gel. At 10Hz, the FDA standard frequency for evaluating cutaneous electrodes[48], we see nearly an order of magnitude drop in impedance with an 88% decrease when compared to the electrolytic gel (p=0.008, two-sample t test). At 100Hz and 1kHz, we see also see a large decrease in impedance corresponding to a 82% and 77% decrease, respectively (p = 0.05 and p = 0.074, two- sample t test).

The reduction in impedance and reduction in phase delay likely arises from the high conductance of the PEDOT:PSS gel when compared to other conducting polymer gels or conventional electrolytic hydrogels[35]. The use of secondary dopant DMSO in the manufacturing process is critical in this case as it enhances the percolation pathways of the conducting polymer network during initial synthesis. The secondary doping with DMSO gives rise to order within PEDOT:PSS on two length scales: (i) transforming colloidal PEDOT:PSS

microgels into linear chains facilitates long range interactions with PSS chain entanglement[49,50] and (ii) short range ordering of PEDOT:PSS due to enhanced π-π stacking between PEDOT-rich domains [51]. As the DMSO is extracted during the long drying process (yielding a pure PEDOT:PSS hydrogel), the order that DMSO lended to the PEDOT:PSS network is preserved, encouraging the formation of crystalline PEDOT-rich nanofibrils and keeping PSS chains entangled[49],[50] allowing the percolationdriven charge transport[51] shown in Figure 1c. The ionic conductance of the PEDOT:PSS gel arises from high water content coupled with the porosity of hydrogel architectures permitting bioconduction ions to easily move through the structure like in biological tissues[49]. Furthermore, the porosity on the surface coupled with the gel's softness (<2 MPa & >30% ultimate strain[35] similar to skin[52],[53],[44]) enables intimate contact between the gel and skin pores. This may speed up the charge transfer kinetics skinelectrode interface to lower impedance.

The electrolytic gel and bare metal case have very similar impedance trends in figure 4a. In practice, dry electrodes have higher impedance[1],[54] primarily due to air gaps creating imperfect contact and the electrode rigidity leading to motion artifacts since the impedance is varying from the imperfect contact along curved skin surfaces[1].

Our novel measure in Figure 2a and Supplementary Figure S2 addresses these issues with an equal pressure planar contact[55],[56]. In addition to lower impedance values, we see consistently lower impedance variability in the form of standard error across all frequencies for the PEDOT:PSS gel (Figure S3) including an order of magnitude lower variability across skin samples at 10Hz, 100Hz and 1khz when compared to both the bare and electrolytic gel cases (corresponding to a >76%, >83%, and >86% decrease, respectively). This lower impedance variability may potentially lead to a higher signal-to-noise ratio in multi-electrode systems due to the balancing of input source impedance for instrumentation amplifiers[42],[57],[58]. We perform these measurements over 5 hours for each condition and find no significant degradation in impedance (Figure 2e).
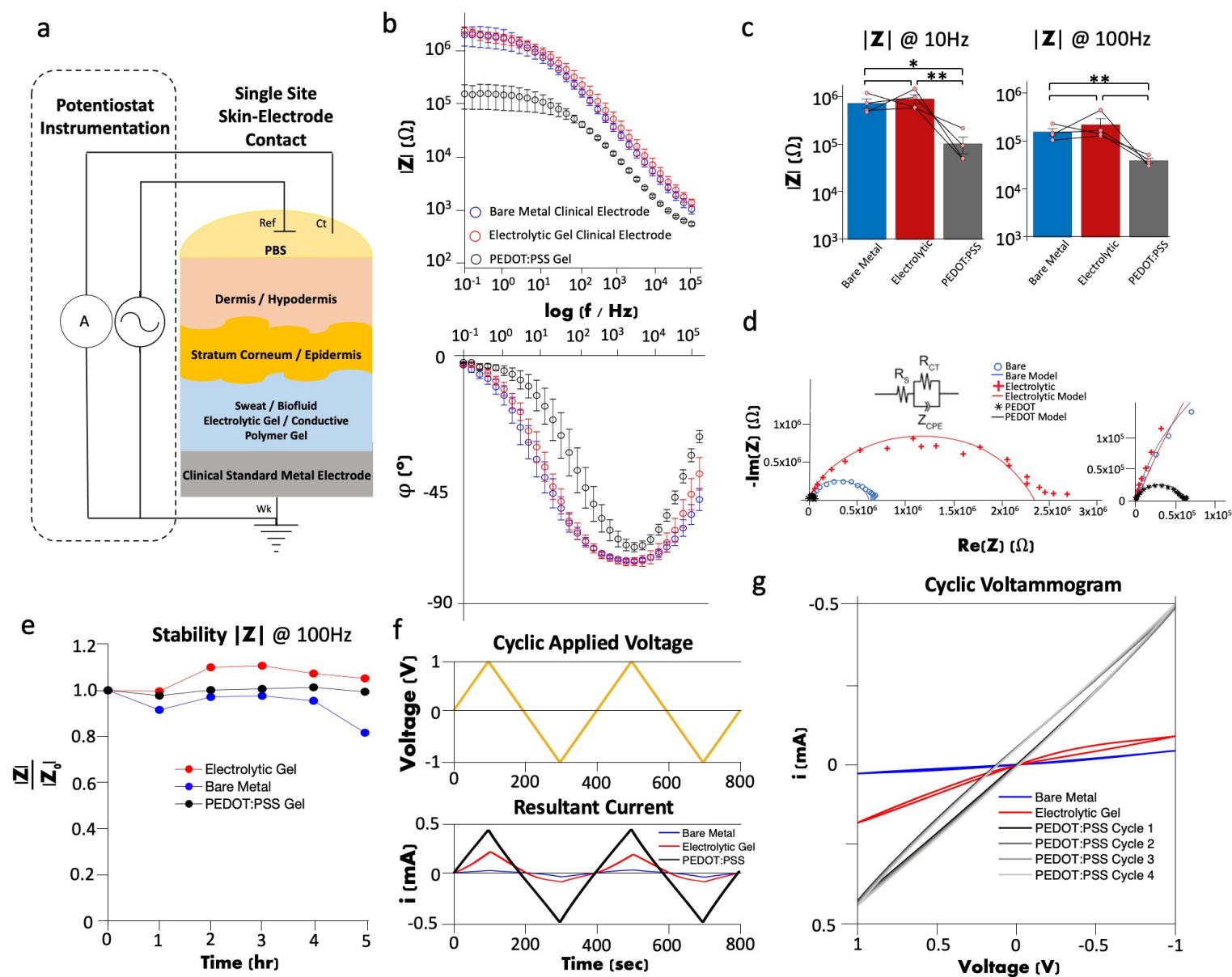
Figure 2: Electrochemical characterization of single site skin-electrode contacts for conductive polymer gels versus clinical electrodes. (a) Schematics showing the interfacial electrochemistry characterized by potentiostat. Ref is the reference electrode, Ct is the counter electrode, and Wk is the working electrode. (b) Bode impedance (top) and phase (bottom) plot for the clinical standard bare metal, electrolytic gel, and the PEDOT:PSS gel. Points are mean with bars representing standard error. (c) Impedance values at various bioelectronic frequencies of interest. Values represent mean with bars representing standard error. n = 4. *, p < 0.05, **, p < 0.01; paired by skin sample t test. (d) Representative Nyquist plot. Fitting from 0.1 Hz to 10 kHz. Zoom in portion on right shows entire frequency spectrum of the PEDOT:PSS case and the high frequency portions for the bare and the electrolytic case (note that these high frequencies are not modeled for the three cases). (e) Impedance stability at 100Hz for the clinical standard bare metal, electrolytic gel, and the PEDOT:PSS gel. Points are mean (n=3). (f) (top) Dynamic potential versus time for cyclic voltammetry. (bottom) Resulting current from applied dynamic potential. (g) Current vs potential for cyclic voltammogram.

2.1.2   Impedance Modeling

To provide insight into the electrochemical performance, two electrical models of skin-electrode impedance are shown in Figure S1. The 3-element Cole-Cole model shown in Figure 2d and on the right of Figure S1 is a simple, general model representing impedance of biological tissues[59],[60] and commonly used to model skin and cutaneous electrodes[10],[55], [61], [41], [62]. Bioelectronic systems present non-ideal capacitive behavior. The constant phase element (CPE) is a fractional-order empirical circuit element used in the Cole-Cole model to fit circuits exhibiting such non-idealities[62],[59],[63],[61],[64]. The impedance of the constant phase element is of the form

$$Z_{CPE}(\omega) = \frac{1}{Q(j\omega)^\alpha}$$

(1)

where $j\omega$ is the imaginary frequency and Q and α are CPE parameters that are independent of frequency. The Cole-Cole model consists of a distribution of Randle's circuits[62], an equivalent circuit model of Faradaic reactions with negligible diffusion, where an ideal capacitor is replaced by the constant phase element as shown in circuit in Figure 2d. The impedance of the Cole-Cole model is

$$Z(\omega) = R_s + \frac{R_{CT}}{1 + R_{CT}Q(j\omega)^\alpha}$$

(2)

where R_s represents the ionic, or Ohmic, resistance, and R_{CT}, represents the charge transfer resistance. The CPE parameters, α and Q, characterize the deviation from ideal capacitance. If $\alpha = 1$, the system is an ideal Faradaic reaction and Q represents the electrical double layer capacitance at the electrochemical interface. If $\alpha < 1$, the interface displays non-ideal capacitive behavior attributed to the surface heterogeneity (such as the varying thickness of skin) or normally distributed time constants (such as differences in resistivity in successive layers of the stratum corneum[62]).

A useful way to conceptualize the Cole-Cole model is to view it as a surface distribution of time constants at the electrode-to-tissue interface shown in Figure 1b. The impedance of the time constant distribution is of the form

$$Z(\omega) = R_s + \frac{R_{CT}}{1 + (j\omega\tau)^\alpha}$$

(3)

Note that equation 2 and 3 are equivalent. However, from the viewpoint of equation 3, τ represents a mean time constant and α represents the depression of a semi-circle in a Nyquist impedance plot of an ideal RC circuit[64]. This viewpoint is especially useful in cutaneous electronics since, in human skin, the constant phase element is representative of the size and/or charge distribution of the eccrine sweat glands that provide DC current through the epidermis[41]. The mean time constant can be easily solved as

$$\tau = (R_{CT}Q)^{\frac{1}{\alpha}}$$

(4)

Mechanistically, it is plausible that the time constants follow a distribution since the electrochemical activation energy is unlikely to have the same value at all points of the electrode surface. Extending this theory, the mean capacitance can be easily calculated as

$$C = \frac{\tau}{R_{CT}}$$

(5)

Figure 2d shows an example Nyquist impedance plot of the three cases as well as the corresponding Cole-Cole model fit. Table S2 summarizes the parameters extracted from the Cole-Cole model fittings. We see for all three cases $\alpha \approx 0.8$, matching reported values to skin[62],[65]. The electrolytic gel displays an order of magnitude larger Ohmic resistance than the bare metal and PEDOT:PSS gel. The bare metal and electrolytic gel have nearly exactly the same value for Q with the PEDOT:PSS gel having an order of magnitude larger Q than the bare metal and electrolytic gel. The electrolytic gel shows an order of magnitude large Ohmic resistance when compared to the bare metal and PEDOT:PSS gel case. The charge transfer resistance of the PEDOT:PSS gel is an order of magnitude lower than both the bare metal and electrolytic gel cases. The time constant, τ, for the bare metal and electrolytic gel are nearly identical at 30ms and 27.8ms, respectively. Compared to the bare metal and electrolytic gel, the PEDOT:PSS gel displays a factor of six lower time constant at 5.12ms. The mean capacitance, C, for the bare metal and electrolytic gel are similar at 14.6μF and 15.7μF, respectively. Compared to the bare metal and electrolytic gel, the PEDOT:PSS gel displays over twice the capacitance at 33.9μF.

The Cole-Cole model parameters allow for insight into why the PEDOT:PSS gel performs better than the clinical electrodes. For bioelectronic processes (and more generally systems with ion-to-electron charge movement), the limiting factor is usually the charge transfer resistance, R_{CT}, due to slow charge transfer kinetics[51] when compared to systems exhibiting only electronic resistances or only electrolytic (ionic) resistances. This behavior was consistent with the fitted Cole-Cole model parameters summarized in Table S2. The reduction in R_S for the PEDOT:PSS gel likely arises from its high electronic conductance compared to conventional hydrogels or other conductive polymers: doping PEDOT with PSS raises its conductance due to more electronic charge carriers in the form of bipolarons[49]. The average charge transfer resistance, R_{CT}, for the PEDOT:PSS gel was over an order of magnitude lower than the electrolytic gel and bare metal case. The PEDOT:PSS gel allows for more seamless current movement by matching ionic conduction at the gel-skin interface with electronic conduction at the gel-electrode interface. These matching of conductance in the pure PEDOT:PSS hydrogel likely speeds up charge transfer kinetics, resulting in a lower time constant, τ, and the increased impedance bandwidth in Figure 2b.

2.1.3 Cyclic Voltammetry

We performed cylic voltammetry measurements[66] from -1V to 1V versus the Ag/AgCl reference electrode at a scan rate of 10mV/s using the same setup in Figure 2a. Cyclic voltammetry allows investigation of the interfacial electrochemical behavior in the time domain as opposed to the frequency domain of EIS[67].

As seen in Figure 2g, the PEDOT:PSS hydrogels present blunt and slanted cyclic voltammograms[67],[68]. This behavior follows Randle's circuit and the Cole-Cole model closely: the slope of the potential vs current curve represents the Ohmic resistance, the area between charging and discharge curves represents the capacitance. Here, the mixed conductivty of the PEDOT:PSS hydrogels becomes evident once again. The higher slope of the PEDOT:PSS hydrogel represents a markedly lower resistance due to the lower charge transfer resistance in conjuction with the lower series resistance as described in Section 2.1.2. The reactions occurring throughout the volume of the PEDOT:PSS hydrogel as seen in Figure 1 lead to a capacitance scaling with the volume of the hydrogel as opposed to the area of the electrode[49],[69]. This leads to a significantly increased capacitance as evidenced by PEDOT:PSS hydrogels' larger area between charging and discharging curves when compared to clinical standard electrodes[49].

2.2 Baseline *In-Vivo* Electromyography

To verify the *ex-vivo* skin-electrode contact impedance reduction translates to higher fidelity biopotential signals, we conducted electromyographic studies on six healthy adult subjects (4 male, 2 female, age=28±5). All subjects consented to an approved Institutional Review Board protocol from Harvard University (IRB #21-0090).

Each subject's skin on forearm, wrist, and elbow was cleaned with an alcohol prep pad and then saline was applied to the measurement site, above the flexor carpi radialis[70] muscle on the forearm. Pregelled clinical Ag/AgCl electrodes (Noraxon) were placed on the measurement site (working electrode), the wrist below the palm (reference electrode), and bony portion of elbow (ground electrode). All electrodes were connected to a biopotential amplifier (BIOPAC) acquiring data at a 2kHz sampling rate with a 1HZ high-pass filter stacked with a 5Hz high-pass filter. Each subject was tasked with completing four to five maximum voluntary isometric contractions (MVIC), a baseline measurement for tracking muscle activation[70],[71]. The MVIC consisted of making and holding a fist at maximum effort for five seconds, followed by a rest period of ten seconds. Following MVIC with the clinical standard control setup, the exact location of the electrode was outlined on the subject to control for placement as seen in Figure 3b.

After measurement with clinical electrodes, we remove the electrolytic gel and cut away the excess foam portions, leaving only bare metal. The metal electrode was immediately adhered to an adhesive stretchable silicone rubber fixation. A PEDOT:PSS hydrogel sample was then placed on the metal electrode within an adhesive stretchable silicone rubber fixation seen in Figure 3a. Fabrication steps for the adhesive fixture can be seen in Supporting Information Section S2. The same skin preparation and test for the clinical electrode was repeated with the PEDOT:PSS gel. Data was notch-filtered offline at 40dB bandstop at 60Hz to remove power line interference noise, followed by a standard EMG high-pass motion artifact filter with a corner frequency of 20Hz and a slope of 12 dB/oct[3]. Root-mean-square (RMS) envelope of the filtered signal was calculated with a 200ms wide moving window[14],[72]. By controlling for using the same metal electrode, same skin location and treatment, we directly compared between electrolytic gel-skin interfaces and conducting polymer gel-skin interfaces. Recording snippets from

three subjects along with the signal-to-noise ratio from the entire recordings are shown in Figure 3c. The PEDOT:PSS hydrogel demonstrated consistently higher SNR compared to pregelled clinical electrodes, results for all subjects summarized in Figure S4. All subjects demonstrated an increase in SNR, with two of the subjects displaying over a 3dB SNR increase, corresponding to twice the output power and bandwidth[73]. The power spectral density (PSD) of the raw electromyographic data reliably demonstrated more power from the PEDOT:PSS hydrogels than the pregelled clinical electrodes across all subjects and all frequencies (Figure 3d). Zooming into only subject 6 (Figure 3d) shows an example PSD for a single subject.
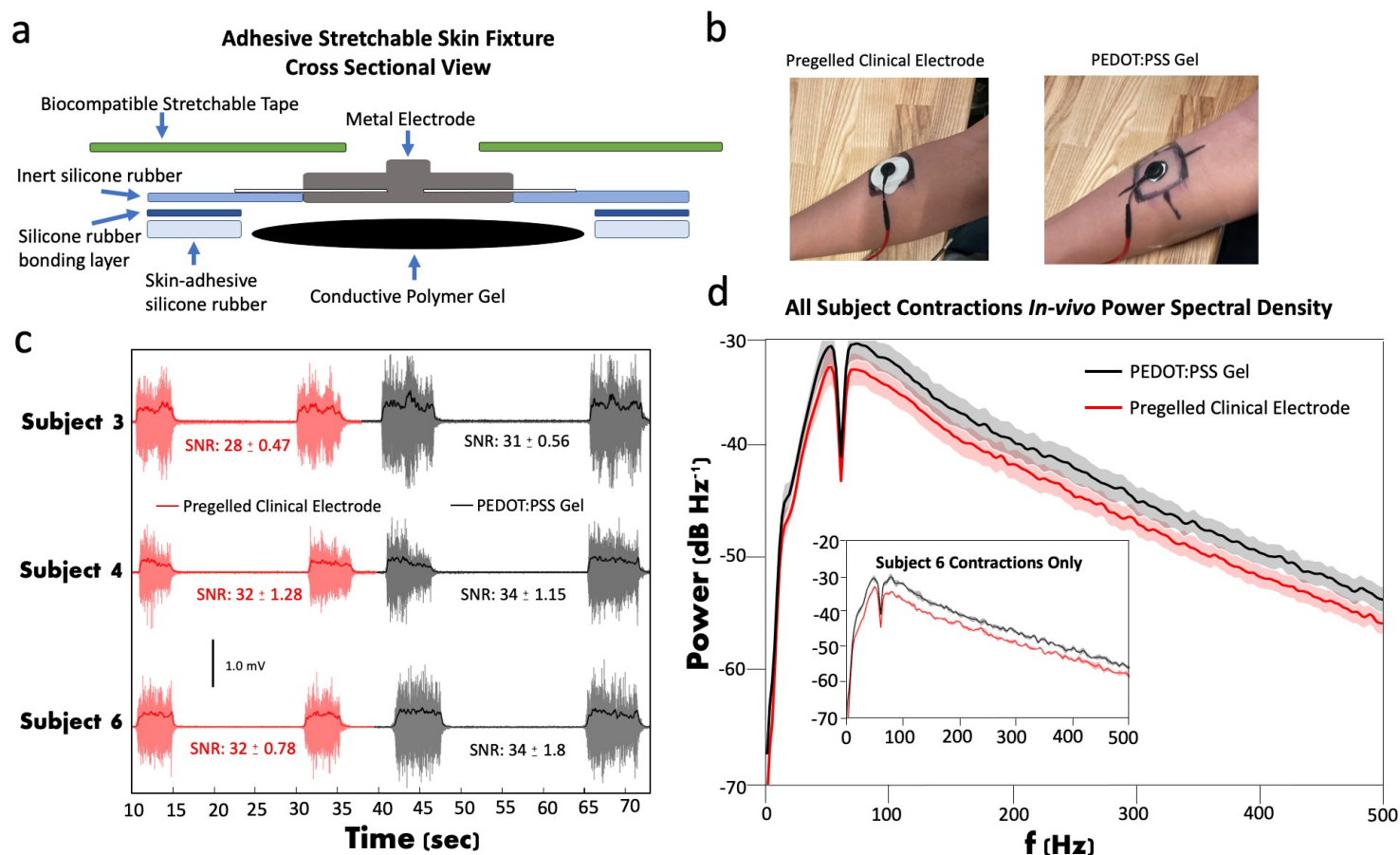

Figure 3: Interfacing and performance of conductive polymer hydrogels to skin for electromyographic recordings. a) An elastomer-based soft stretchable adhesive structure used to couple the free-standing conductive polymer hydrogel to skin. b) Experimental setup for the voluntary contraction task. The pregelled clinical electrode and PEDOT:PSS gel electrode are placed on the same forearm location for the task. Clinical pregelled electrodes are placed on the elbow and wrist (both not shown), as ground and reference electrodes, respectively. c) Example electromyography recordings for three subjects. The data is shown as a transparent red and a transparent grey for clinical electrodes and PEDOT:PSS gel electrodes, respectively. The RMS envelope are overlaid in dark red and in black for the clinical electrodes and PEDOT:PSS gel electrodes, respectively. The signal-to-noise ratios for each subjects entire recording appear below the data for each subject, with red corresponding to clinical pregelled electrodes and black corresponding to PEDOT:PSS hydrogels. d) Power spectral density plots for all subjects' contractions. Values represent mean with shading representing standard error. Inset presents power spectral density of a single subject.

2.3 Applications in Real-Time Robotic Control

By coupling the PEDOT:PSS hydrogel to the human via the soft adhesive skin fixture in Figure 3a, we utilize PEDOT:PSS gels as the sole bioelectronic sensor in an integrated system. We take advantage of the PEDOT:PSS hydrogel's lower impedance and higher signal-to-noise ratio to demonstrate the sensors can provide adequate enough signal control for real-time robotic control with a human-in-the-loop. Specifically, we use the PEDOT:PSS gels in a bipolar arrangement on the forearm in a robotic neural interface system seen in Figure 4. The myoelectric signal activation is mapped to a velocity control signal for a robot arm along a preset path to complete an activity of daily living: pick-and-place. The user does not need to move their joints to enable this control, only provide varying grades of natural muscle activation, potentially opening this design to users without fine motor control and/or pain and difficulty moving their joints such as those with arthritis[74].

The system architecture of our interface is in Figure S5. A computer running the Robot Operating System (ROS) interfacing with a UR5e robot arm reads in data from a simple commercial microcontroller (Arduino Uno) acquiring raw data at 1kHz from the same biopotential amplifer used in the previously described electromyography recordings. The microcontroller runs real-time digital signal processing algorithms to run similar filtering algorithms done offline in the previous section. Specifically, we implemented 1) a 60Hz notch filter, 2) a 20Hz-250Hz bandpass filter, and 3) a root-mean-square function with a 200ms window. The commanded velocities are relative velocities ranging from 0 to 1, where 0 is no movement and 1 is maximum velocity along the preset path. The paths and velocities are commanded with the use of freely available open-source software[75],[76]. Supplmentary Video 1 and Figure 4 demonstrate our implementation. The pure PEDOT:PSS hydrogels enable sensitive real-time robotic myoelectric control with simple calibration. The use of myoelectric signals in robotics is a topic of great interest for safe compliant human-robot interaction[77], prosthetic control[78], and intuitive teleoperated robot control for environments too dangerous for a human[79].

3 Conclusion

This study demonstrates the use of a conductive polymer hydrogel as a cutaneous electrode on a human being. The favorable electrochemical interfacial behavior promised by the PEDOT:PSS hydrogel's mixed ionic-electronic conduction resulted in dramatically reduced skin-electrode contact impedance across all frequencies in a pre-clinical *ex-vivo* model. At 10Hz, the FDA standard frequency for evaluation of skin electrodes, we demonstrate nearly an order of magnitude (88%) drop in impedance. We complement the straight-forward fabrication[35] of the PEDOT:PSS hydrogel by providing facile manufacturing of an elastomer-based adhesive stretchable skin fixture to couple the PEDOT:PSS hydrogel to human skin. The PEDOT:PSS hydrogel displays improved signal-to-noise-ratio in *in-vivo* EMG recordings compared to clinical electrolytic gelled electrodes. As a final demonstration of the PEDOT:PSS hydrogel's utility in cutaneous electronics, we use it as the sensor for a human-robot interface where the user finely controls robot velocity in a pick-and-place task where using only their natural myoelectric contractions. This work provides a sound basis for the use of PEDOT:PSS hydrogels as a sensing modality for cutaneous bioelectronic recordings. We envision future integration of these conductive polymer hydrogels into more robust integrated wearable systems could open new avenues for coupling man and machine.
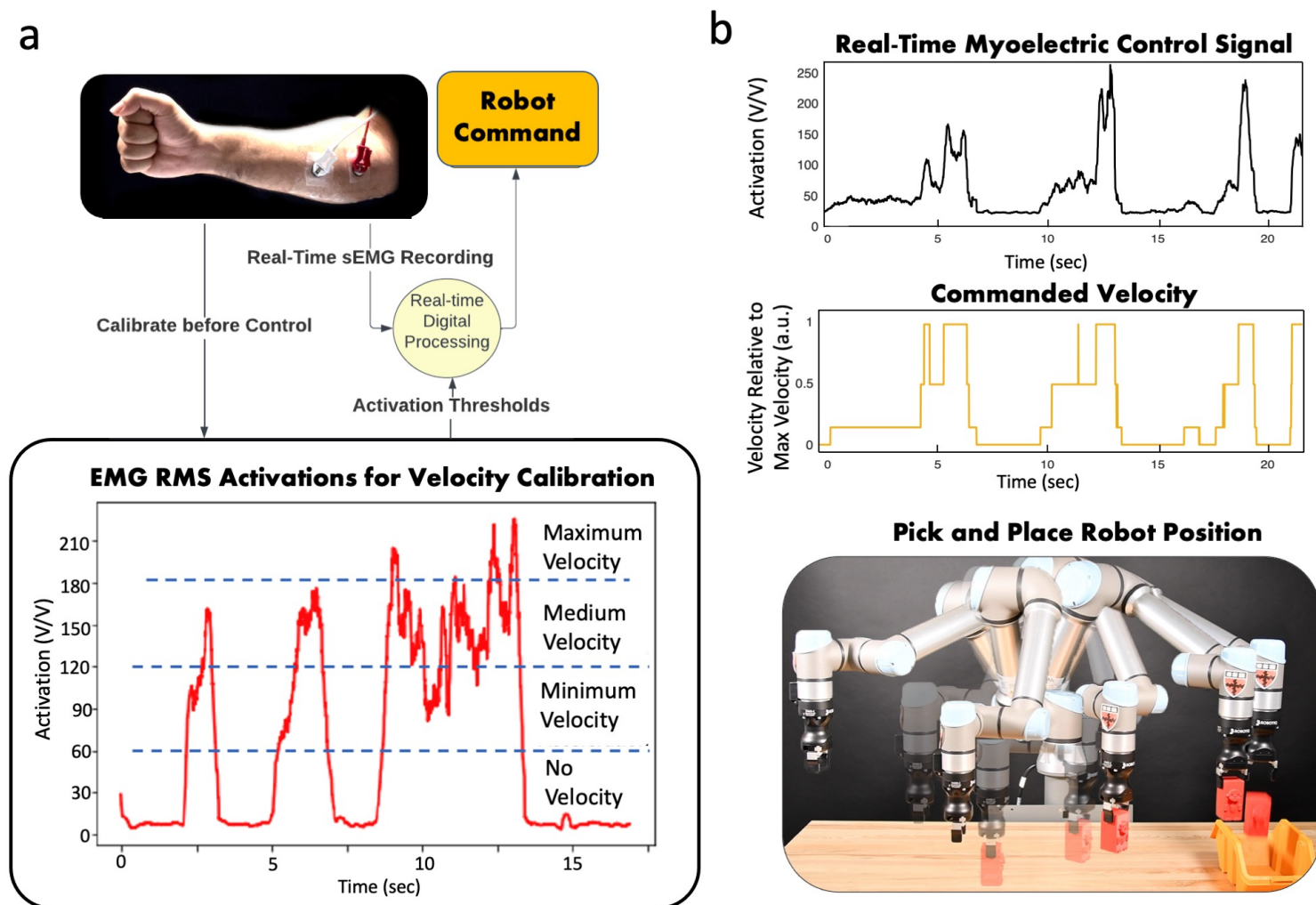
a

b

Figure 4: Conductive polymer hydrogel cutaneous electrodes enable real-time myoelectric velocity control of a robotic pick-and-place task. a) Flowchart of how to use conductive polymer hydrogels in the designed robotic system. A user first calibrates their muscle activation (in the form of RMS envelope) to desired velocities. After calibration, the integrated system combines real-time digital signal processing on a hobbyist microcontroller with the bioamplifier recording to command the robot's velocity along a pre-programmed path. The full system architecture can be seen in Figure S5. b) Example control of a robot. See Video S1 for full live recording with real-time data plotting. (top) Recorded myoelectric signals. (middle) Corresponding velocity signals to robot. In this calibration, EMG activations of 30, 50, and 90, map to relative velocity commands of 0.15, 0.5, and 1, respectively. (bottom) Robot position along the pick-and-place task.

4   Experimental Section

Fabrication of Pure PEDOT:PSS Hydrogels: PEDOT:PSS aqueous solution (1.1 wt% in H2O, surfactantfree, high-conductivity grade, Clevios PH 1000, MSE Supplies, Tucson, AZ) was vigorously homogenized using ultrasonic treatment (20'@80% amplitude, Q500 Sonicator, Qsonica, Newtown, USA) for 20 minutes with a 75% duty cycle both upon arrival and after any storage before use. Dimethyl sulfoxide (DMSO, 472301, Sigma-Aldrich, St. Louis, USA) was added in 13 vol.% of the final solution. The solution was mixed at 2000 RPM and degassed at 2200 RPM using a planetary centrifugal mixer (ARE-310, Thinky USA, Laguna Hills, U.S.A.) for 10 minutes each. The mixed solution was solvent casted in 3D printed wells (VeroWhite or Durus, Stratasys, Rehovot, Israel) covered with teflon (Non-Stick Dry Film Lubricant Aerosol 100% Teflon Spray, DuPont, Wilmington, USA). The samples were then dried for 36 hours at 70C. Following annealing and hydration as described by Lu et al.[35], the samples were cut out from the wells with a hole punch and taken out with tweezers.

    Single Contact Skin-Electrode Interface Electrochemical Impedance Spectroscopy: Electrochemical impedance spectroscopy (EIS) measurements ranged from 0.1 to 10^5 Hz. Each measurement contained three frequency sweeps using a sinusoidal voltage, 10mV peak-to-peak amplitude. We used an aqueous Ag/AgCl electrode as the reference electrode and a platinum electrode as the counter electrode. The PEDOT:PSS gel and the clinical standard methods measurements both used a clinical Ag/AgCl EMG electrode (Noraxon USA, Scottsdale, U.S.A.) as the working electrode and alternated between using the pre-gelled electrolyte gel, the PEDOT:PSS gel, and no gel (i.e. bare) for the EIS configuration in Figure 2a and Figure S2.

    We conducted measurements using an EIS system (SP-150 potentiostat/galvanostat and EC-Lab Software, BioLogic USA, Knoxville, U.S.A.). The porcine skin samples were approximately 10 cm x 10 cm, 2-5 mm thick, taken from the upper portions of the forelimbs as well as lower chest and upper abdomen. The specimens were stored at approximately 4°C in saline immediately after harvest. Measurements were conducted within seven days of harvesting. Before measurement, the epidermal side of the skin was lightly blotted with a paper towel to remove any excess saline droplets and then wiped clean with an alcohol wipe. During measurements, the samples were pressed between two acrylic plates to ensure equal pressure and planar contact between sample and electrode.

    Single Contact Skin-Electrode Interface Cyclic Voltammetry: Using the same setup as the EIS measurements, cyclic voltammetry (CV) measurements ranged from -1V to 1V with respect to the reference electrode with a scan rate of 10mV/s.
    The same porcine skin samples and potentiostat for EIS were used for CV.

    Impedance Modeling: We modeled from 0.1Hz to 10kHz. 10kHz is already an order of magnitude above bioelectronic frequencies, the stratum corneum dominates the impedance of the skin below 10kHz[60], and above 10kHz ideal instrumentation assumptions regarding the gain in the potentiostat's amplification start to break down and compound with other high frequency error sources such as thermal fluctuations of resistivity and concentration of species[80]. We fit the model using the EC-Lab software. We optimized the fit using the Levenberg-Marquardt algorithm with 10,000 random seeds for the initial condition.

    Electromyography Recordings: All electrodes were connected to a research-grade biopotential amplifier (MP35, BIOPAC Systems, Inc., Goleto, USA) acquiring data at 2kHz with a 1Hz high-pass filter stacked witha 5Hz high-pass filter. Recording electrodes were placed on the flexor carpi radialis muscle with pregelled Noraxon electrodes used as the reference electrode and the ground electrode placed on the wrist below the

palm and on the bony portion of the elbow, respectively. All offline processing and data analysis were completed with custom scripts developed in MATLAB. Data was notch-filtered offline with 40dB bandstop at 60Hz to remove noise from power line interference, followed by a standard EMG highpass motion artifact filter with a corner frequency of 20Hz and a slope of 12 dB/oct. RMS envelope of the filtered signal was calculated with a 200ms wide moving window. The SNR was calcu lated using the builtin SNR function in MATLAB where the signal was the 5 seconds of MVIC contraction and the noise was the time during no activation, i.e. rest. The power spectral density was calculated using Welch's method in MATLAB (function pwelch) on the data received from the biopotential amplifier following 60Hz filtering with a window size of 500 points, overlap of 250 points, and 1000 discrete Fourier transform (DFT) points. All subjects consented to an approved Institutional Review Board protocol from Harvard University (IRB #21-0090).

Robotic Control: The full system architecture can be see in Figure S5. A computer running Ubuntu 20.04 and ROS Noetic interfaces with a UR5e robot arm fit with a Robotiq gripper. An Arduino Uno runs a reads in raw data from the BIOPAC biopotential amplifier used for the electromyographic recordings. The raw data is then online processed on the Arduino at 1kHz using digital signal processing algorithms written in the C programming language. Specifically, we implemented in real-time: 1) a discrete time 60Hz notch filter (Bandstop butterworth filter, order=2, alpha1=0.058, alpha2=0.062), 2) a discrete time 20Hz-250Hz bandpass filter using the bilinear transform, and 3) a root-mean-square function with a 200ms window using circular buffers for fast summing operations. This processed data is then published by the Arduino to a ROS Node which is then read by a custom Python script running a ROS subscriber node. The custom Python script runs a preset pick-and-place trajectory of the robot arm and commands velocity. The commanded velocity is mapped from the processed EMG signals sent from the Arduino.

Statistical Analysis: Experimental data for sections 2.1 were arranged in Microsoft Excel Software and further analyzed in MATLAB. p-values were determined with two-sample t-tests performed in MATLAB with function ttest2. *, $p < 0.05$, **, $p < 0.01$. Section 2.2 and 2.3 were analyzed directly in MATLAB. Data for 2.1 and 2.2 were plotted as mean ± standard error of mean (SEM).

Supporting Information

Supporting Information is available from the Wiley Online Library or from the author.

Acknowledgements

References

[1] J. Heikenfeld, A. Jajack, J. Rogers, P. Gutruf, L. Tian, T. Pan, R. Li, M. Khine, J. Kim, J. Wang, *Lab on a Chip* **2018**, *18*, 2 217.

[2] A. G. Correa, E. Laciar, H. Patin˜o, M. Valentinuzzi, In *Journal of Physics: Conference Series*, volume 90. IOP Publishing, **2007** 012081.

[3] C. J. De Luca, L. D. Gilmore, M. Kuznetsov, S. H. Roy, *Journal of biomechanics* **2010**, *43*, 8 1573.

[4] Y. Luo, R. H. Hargraves, A. Belle, O. Bai, X. Qi, K. R. Ward, M. P. Pfaffenberger, K. Najarian, *The Scientific World Journal* **2013**, *2013*.

[5] R. Castrillo´n, J. J. P´erez, H. Andrade-Caicedo, *Biomedical engineering online* **2018**, *17*, 1 38.

[6] F. Ershad, A. Thukral, J. Yue, P. Comeaux, Y. Lu, H. Shim, K. Sim, N.-I. Kim, Z. Rao, R. Guevara, et al., *Nature communications* **2020**, *11*, 1 1.

[7] K. E. Mathewson, T. J. Harrison, S. A. Kizuk, *Psychophysiology* **2017**, *54*, 1 74.

[8] B. B. Murphy, P. J. Mulcahey, N. Driscoll, A. G. Richardson, G. T. Robbins, N. V. Apollo, K. Maleski, T. H. Lucas, Y. Gogotsi, T. Dillingham, et al., *Advanced Materials Technologies* **2020**, *5*, 8 2000325.

[9] F. Stauffer, M. Thielen, C. Sauter, S. Chardonnens, S. Bachmann, K. Tybrandt, C. Peters, C. Hierold, J. Vo¨ro¨s, *Advanced healthcare materials* **2018**, *7*, 7 1700994.

[10] S. Yao, W. Zhou, R. Hinson, P. Dong, S. Wu, J. Ives, X. Hu, H. Huang, Y. Zhu, *Advanced Materials Technologies* **2022**, 2101637.

[11] A. Lipatov, H. Lu, M. Alhabeb, B. Anasori, A. Gruverman, Y. Gogotsi, A. Sinitskii, *Science advances* **2018**, *4*, 6 eaat0491.

[12] D. Pani, A. Dess`ı, J. F. Saenz-Cogollo, G. Barabino, B. Fraboni, A. Bonfiglio, *IEEE Transactions on Biomedical Engineering* **2015**, *63*, 3 540.

[13] P. Leleux, C. Johnson, X. Strakosas, J. Rivnay, T. Herv´e, R. M. Owens, G. G. Malliaras, *Advanced healthcare materials* **2014**, *3*, 9 1377.

[14] T. Roberts, J. B. De Graaf, C. Nicol, T. Herv´e, M. Fiocchi, S. Sanaur, *Advanced healthcare materials* **2016**, *5*, 12 1462.

[15] K. Nagamine, S. Chihara, H. Kai, H. Kaji, M. Nishizawa, *Sensors and Actuators B: Chemical* **2016**, *237* 49.

[16] I. B. Dimov, A. Sautter, W. L¨ovenich, C. Neumann, G. G. Malliaras, *Applied Physics Reviews* **2022**, *9*, 2 021401.

[17] L. Zhang, K. S. Kumar, H. He, C. J. Cai, X. He, H. Gao, S. Yue, C. Li, R. C.-S. Seet, H. Ren, et al., *Nature communications* **2020**, *11*, 1 1.

[18] P. Tan, H. Wang, F. Xiao, X. Lu, W. Shang, X. Deng, H. Song, Z. Xu, J. Cao, T. Gan, et al., *Nature communications* **2022**, *13*, 1 1.

[19] H. Yuk, B. Lu, S. Lin, K. Qu, J. Xu, J. Luo, X. Zhao, *Nature communications* **2020**, *11*, 1 1.

[20] D. Khodagholy, J. N. Gelinas, Z. Zhao, M. Yeh, M. Long, J. D. Greenlee, W. Doyle, O. Devinsky, G. Buzs´aki, *Science Advances* **2016**, *2*, 11 e1601027.

[21] A. C. Paulk, J. C. Yang, D. R. Cleary, D. J. Soper, S. H. Lee, M. Ganji, Y. G. Ro, H. Oh, L. Hossain, N. Rogers, et al., *bioRxiv* **2019**, 770743.

[22] V. R. Feig, H. Tran, M. Lee, Z. Bao, *Nature communications* **2018**, *9*, 1 1.

[23] T. Zhou, H. Yuk, F. Hu, J. Wu, F. Tian, H. Roh, Z. Shen, G. Gu, J. Xu, B. Lu, et al., *bioRxiv* **2022**.

[24] Q. Wang, X. Pan, C. Lin, D. Lin, Y. Ni, L. Chen, L. Huang, S. Cao, X. Ma, *Chemical Engineering Journal* **2019**, *370* 1039.

[25] S. Xu, T. Li, H. Ren, X. Mao, X. Ye, B. Liang, In *2020 IEEE SENSORS*. IEEE, **2020** 1–4.

[26] Y. Wang, Z. Qu, W. Wang, D. Yu, *Colloids and Surfaces B: Biointerfaces* **2021**, *208* 112088.

[27] F. Fu, J. Wang, J. Yu, *Journal of Materials Chemistry C* **2021**, *9*, 35 11794.

[28] J.-C. Hsieh, H. Alawieh, Y. Li, F. Iwane, L. Zhao, R. Anderson, S. I. Abdullah, K. W. K. Tang, W. Wang, I. Pyatnitskiy, et al., *Biosensors and Bioelectronics* **2022**, *218* 114756.

[29] C. Lim, Y. J. Hong, J. Jung, Y. Shin, S.-H. Sunwoo, S. Baik, O. K. Park, S. H. Choi, T. Hyeon, J. H. Kim, et al., *Science Advances* **2021**, *7*, 19 eabd3716.

[30] M. A. Bhat, R. A. Rather, A. H. Shalla, *Synthetic Metals* **2021**, *273* 116709.

[31] H. Yang, S. Ji, I. Chaturvedi, H. Xia, T. Wang, G. Chen, L. Pan, C. Wan, D. Qi, Y.-S. Ong, et al., *ACS Materials Letters* **2020**, *2*, 5 478.

[32] X. Liu, X. Chen, X. Chi, Z. Feng, C. Yang, R. Gao, S. Li, C. Zhang, X. Chen, P. Huang, et al., *Nano Energy* **2022**, *92* 106735.

[33] F. Fu, J. Wang, H. Zeng, J. Yu, *ACS Materials Letters* **2020**, *2*, 10 1287.

[34] H. Ma, J. Hou, W. Xiong, Z. Zhang, F. Wang, J. Cao, P. Jiang, H. Yang, X. Liu, J. Xu, In *International Conference on Intelligent Robotics and Applications*. Springer, **2022** 295–304.

[35] B. Lu, H. Yuk, S. Lin, N. Jian, K. Qu, J. Xu, X. Zhao, *Nature communications* **2019**, *10*, 1 1.

[36] S. Maji, J. Dookhy, M. J. Burke, *Measurement: Sensors* **2021**, *15* 100044.

[37] A. Albulbul, *Bioengineering* **2016**, *3*, 3 20.

[38] E. Bihar, T. Roberts, Y. Zhang, E. Ismailova, T. Herv´e, G. G. Malliaras, J. B. De Graaf, S. Inal, M. Saadaoui, *Flexible and Printed Electronics* **2018**, *3*, 3 034004.

[39] N. Celik, N. Manivannan, A. Strudwick, W. Balachandran, *Nanomaterials* **2016**, *6*, 9 156.

[40] M. K. Yapici, T. Alkhidir, Y. A. Samad, K. Liao, *Sensors and Actuators B: Chemical* **2015**, *221* 1469.

[41] M. E. Orazem, P. Shukla, M. A. Membrino, *Electrochimica Acta* **2002**, *47*, 13-14 2027.

[42] D. Prutchi, M. Norris, *Design and development of medical electronic instrumentation: a practical perspective of the design, construction, and test of medical devices*, John Wiley & Sons, **2005**.

[43] M. Bariya, L. Li, R. Ghattamaneni, C. H. Ahn, H. Y. Y. Nyein, L.-C. Tai, A. Javey, *Science advances* **2020**, *6*, 35 eabb8308.

[44] H. Joodaki, M. B. Panzer, *Proceedings of the Institution of Mechanical Engineers, Part H: Journal of Engineering in Medicine* **2018**, *232*, 4 323.

[45] F. Meurens, A. Summerfield, H. Nauwynck, L. Saif, V. Gerdts, *Trends in microbiology* **2012**, *20*, 1 50.

[46] A. Summerfield, F. Meurens, M. E. Ricklin, *Molecular immunology* **2015**, *66*, 1 14.

[47] T. P. Sullivan, W. H. Eaglstein, S. C. Davis, P. Mertz, *Wound repair and regeneration* **2001**, *9*, 2 66.

[48] FDA-2019-D-1649: Cutaneous electrodes for recording purposes – performance criteria for safety and performance based pathway, URL https://www.regulations.gov/docket/FDA-2019-D-1649.

[49] H. Yuk, B. Lu, X. Zhao, *Chemical Society Reviews* **2019**, *48*, 6 1642.

[50] H. Shi, C. Liu, Q. Jiang, J. Xu, *Advanced Electronic Materials* **2015**, *1*, 4 1500017.

[51] K. Wijeratne, U. Ail, R. Brooke, M. Vagin, X. Liu, M. Fahlman, X. Crispin, *Proceedings of the National Academy of Sciences* **2018**, *115*, 47 11899.

[52] M. Pawlaczyk, M. Lelonkiewicz, M. Wieczorowski, *Advances in Dermatology and Allergology/Postepy Dermatologii i Alergologii* **2013**, *30*, 5 302.

[53] M. Griffin, B. Leung, Y. Premakumar, M. Szarko, P. Butler, *Journal of Otolaryngology-Head & Neck Surgery* **2017**, *46*, 1 1.

[54] G. Li, S. Wang, Y. Y. Duan, *Sensors and Actuators B: Chemical* **2017**, *241* 1244.

[55] B. Taji, A. D. Chan, S. Shirmohammadi, *IEEE Transactions on Instrumentation and Measurement* **2018**, *67*, 8 1900.

[56] D. J. Hewson, J.-Y. Hogrel, Y. Langeron, J. Duchˆene, *Journal of Electromyography and Kinesiology* **2003**, *13*, 3 273.

[57] P. Horowitz, W. Hill, *The Art of Electronics*, Cambridge Univ. Press, **1989**.

[58] C. Kitchin, L. Counts, *A designer's guide to instrumentation amplifiers*, Analog Devices, **2000**.

[59] F. Clemente, P. Arpaia, C. Manna, *Measurement* **2013**, *46*, 9 3494.

[60] S. Grimnes, O. G. Martinsen, *Bioimpedance and bioelectricity basics*, Academic press, **2011**.

[61] G. Medrano, A. Ubl, N. Zimmermann, T. Gries, S. Leonhardt, In *13th International Conference on Electrical Bioimpedance and the 8th Conference on Electrical Impedance Tomography*. Springer, **2007** 260–263.

[62] B. Hirschorn, M. E. Orazem, B. Tribollet, V. Vivier, I. Frateur, M. Musiani, *Electrochimica acta* **2010**, *55*, 21 6218.

[63] J. B. Allen, R. F. Larry, *Electrochemical methods fundamentals and applications*, John Wiley & Sons, **2001**.

[64] J. R. Macdonald, E. Barsoukov, *History* **2005**, *1*, 8 1.

[65] R. T. Tregear, *Physical functions of skin*, volume 5, Academic Press, **1966**.

[66] N. Elgrishi, K. J. Rountree, B. D. McCarthy, E. S. Rountree, T. T. Eisenhart, J. L. Dempsey, *Journal of chemical education* **2018**, *95*, 2 197.

[67] T. S. Mathis, N. Kurra, X. Wang, D. Pinto, P. Simon, Y. Gogotsi, *Advanced Energy Materials* **2019**, *9*, 39 1902007.

[68] D. Boonpakdee, C. F. G. Y´evenes, W. Surareungchai, et al., *Journal of Materials Chemistry A* **2018**, *6*, 16 7162.

[69] H. Yuk, J. Wu, X. Zhao, *Nature Reviews Materials* **2022**, 1–18.

[70] M. Barbero, R. Merletti, A. Rainoldi, *Atlas of muscle innervation zones: understanding surface electromyography and its applications*, Springer Science & Business Media, **2012**.

[71] P. Konrad, *A practical introduction to kinesiological electromyography* **2005**, *1*, 2005 30.

[72] M. G. Asogbon, O. W. Samuel, Y. Geng, S. Chen, D. Mzurikwao, P. Fang, G. Li, In *2018 IEEE International Conference on Cyborg and Bionic Systems (CBS)*. IEEE, **2018** 576–580.

[73] A. Mojahed, L. A. Bergman, A. F. Vakakis, *Journal of Sound and Vibration* **2022**, 117010.

[74] L. F. Callahan, R. H. Brooks, J. A. Summey, T. Pincus, *Arthritis & Rheumatism: Official Journal of the American College of Rheumatology* **1987**, *30*, 6 630.

[75] UniversalRobots, Universal robots ros driver, URL https://github.com/UniversalRobots/Universal Robots ROS Driver.

[76] C. T. PhD, simple ur move, https://github.com/cbteeple/simple ur move, **2022**.

[77] M. Ison, P. Artemiadis, In *2015 IEEE International Conference on Rehabilitation Robotics (ICORR)*. IEEE, **2015** 416–421.

[78] S. H. Yeon, T. Shu, H. Song, T.-H. Hsieh, J. Qiao, E. A. Rogers, S. Gutierrez-Arango, E. Israel, L. E. Freed, H. M. Herr, *IEEE Transactions on Medical Robotics and Bionics* **2021**, *3*, 3 563.

[79] Y. Yu, J. Li, S. A. Solomon, J. Min, J. Tu, W. Guo, C. Xu, Y. Song, W. Gao, *Science Robotics* **2022**, *7*, 67 eabn0495.

[80] S. Carson, M. Orazem, O. Crisalle, L. Garcia-Rubio, *Journal of the Electrochemical Society* **2003**, *150*, 10 E477.